Microelectronic Engineering xxx (2013) xxx–xxx

Contents lists available at SciVerse ScienceDirect

Microelectronic Engineering

journal homepage: www.elsevier.com/locate/mee

Magnetic flux concentration at micrometer scale

Xu Sun *, Lijun Jiang, Philip W.T. Pong [1]

Department of Electrical and Electronic Engineering, The University of Hong Kong, Hong Kong

ARTICLE INFO

Article history:
Available online xxxx

Keywords:
Magnetic flux concentration
Magnetoresistive sensors
Magnetic gain
Finite element method

ABSTRACT

This paper presents the study of magnetic flux concentration phenomenon of magnetic flux concentrators (MFCs) at the micrometer scale. The main physical principles of magnetic flux concentration were studied by using analytical calculations and finite element method (FEM) simulations. The dependences of achievable maximum magnetic gain on the three critical parameters were analyzed. It shows that material, aspect ratio, and shape are three critical parameters for designing MFCs. Three typical MFCs were designed for magnetoresistive (MR) sensors in applications. The magnetic gain and linear working range of the MFCs were studied and compared. By using the same high-permeability magnetic material (nickel–iron alloy, $\mu_r \approx 10^4-10^5$), the MFCs of different geometries perform differently in magnetic amplification. The T-shaped concentrator shows higher magnetic amplification with magnetic gain $G = 56$ but comparatively narrower linear working range of 1.6 mTesla. The bar-shaped concentrator occupies smaller space and provides 62.5% wider linear working range (2.6 mTesla) than the T-shaped concentrator but at the expense of 32.1% smaller magnetic gain ($G = 38$). In the respect of magnetic gain, the triangle-shaped concentrator *($G = 51$)* is comparable with the T-shaped concentrator. It provides a 42.3% wider linear working range (3.7 mTesla) than the bar-shaped concentrator.

© 2013 Elsevier B.V. All rights reserved.

1. Introduction

This study is motivated by developing a set of principles to guide the design of magnetic flux concentrators (MFCs) for magnetoresistive (MR) sensors. MR sensors offer a flat frequency response from DC to MHz magnetic field signals. This significant advantage makes them attractive for multi-frequency current measurement, such as measuring currents via sensing the magnetic field in printed circuit boards [1], deep-flaw detection and depth profiling eddy current detection in nondestructive evaluation [2,3]. Nowadays, MR sensors are fabricated with the dimension of micrometer by CMOS technology [4,5]. They can be integrated with MFCs, which are on-chip fabricated. The MFCs only intensify the magnetic field in the sensing direction of MR sensor to increase the sensor's sensitivity and achieve noise reduction [6–8]. As such, the MR sensor with enhanced sensitivity can accurately detect an ultralow magnetic field, which varies between a few nanoTesla to a few microTesla. Although works have been done for studying the sensitivity of the macro-scale magnetic sensors combined with MFCs [9], the situations are different in the scenario of micro-scale. At the micrometer scale, the relative sizes of MFCs (e.g. 100 μm) can be made to be multiple orders of magnitude larger than the sizes of MR sensors (e.g. 1 μm). It is possible to design a MFC with very large aspect ratio. Such scenarios are not feasible at the macro-scale. Additionally, there are relatively few research studies on providing a set of general principles of MFC design, particularly for MR sensors with the dimension of micrometer. For the above reasons, a full study is required for providing the physical principles of magnetic flux concentration particularly for MR sensors. Under the guidance of these principles, one can design MFCs with optimized parameters for applications.

In this paper, the physical model of magnetic flux concentration of MFCs was established. The analytical solution of magnetic gain was derived for an elliptical concentrator and a cylindrical concentrator. With the physical models, we investigated the physical principles of magnetic flux concentration. The dependence of magnetic gain on material, aspect ratio, and shape of a MFC was studied. These revealed principles and dependence were then applied to design several typical types of MFCs to be used in practice with MR sensors. The performance of these MFCs was analyzed and discussed.

2. Analytical model of magnetic flux concentration

High-permeability materials immersed into a uniform external magnetic field $\mathbf{H}_0$ tend to attract and concentrate magnetic flux lines. As a result, the magnetic field $\mathbf{H}$ inside the material is amplified. The magnetic flux density $\mathbf{B}$ is related to $\mathbf{H}$ by the relation:

$$\mathbf{B} = \mu_0(\mathbf{H} + \mathbf{M}) = \mu_0(\mathbf{1} + \chi)\mathbf{H} \quad (1)$$

* Corresponding author.
E-mail addresses: sunxu@eee.hku.hk (X. Sun), ppong@eee.hku.hk (P.W.T. Pong).
[1] Tel.: +852 2857 8491; fax: +852 2559 8738.

0167-9317/$ - see front matter © 2013 Elsevier B.V. All rights reserved.
http://dx.doi.org/10.1016/j.mee.2013.01.063

where μ_0 is the vacuum permeability, **M** is the magnetization of the material, and χ_v is the volume magnetic susceptibility. The volume magnetic susceptibility is related to the relative permeability μ_r of the material by $\chi_v = \mu_r - 1$. The inside magnetic field is the result of external field $\mathbf{H}_0$ adding demagnetizing component $\mathbf{H}_d$, $H = \mathbf{H}_0 + \mathbf{H}_d$ For a magnetic object (assuming its material is homogeneous, linear, and isotropic) with a specific shape, for example, an ellipsoid having principle axes in *x*, *y*, and *z* direction, $\mathbf{H}_d$ is related to **M** by [10]:

$$(\mathbf{H_d})_\mathbf{k} = -\mathbf{N_k}\mathbf{M_k} \tag{2}$$

with $k = x, y, z$ where N_k is the demagnetizing factor. As a result, we have

$$\mathbf{H}_k = (\mathbf{H}_0)_k - N_k \chi_v \mathbf{H}_k \tag{3}$$

The inside magnetic field is affected by N_k which entirely depends on the geometry of the object, while χ_v is a material property.

In the case of a rod-shaped magnetic object with a high relative permeability, subjected to a uniform external magnetic field parallel with its axis (*x*-axis), it concentrates the magnetic flux lines into itself. Fig. 1(a) shows the finite element method (FEM) simulation of the concentrated magnetic flux lines with the rod-shaped magnetic object. In the rod, the magnetic field is more concentrated comparing to the environmental field. The rod-shaped magnetic object can be used as a magnetic flux concentrator (MFC) for flux concentration. Fig. 1(b) shows the magnetic gain as a function of the position along the axis from the left end to the right end of the rod-shaped concentrator. It is found that the maximum value of magnetic gain is obtained in the center region of the rod. Since the intensified magnetic field inside the rod-shaped concentrator cannot be directly utilized, the magnetic sensors are usually placed in the vicinity of the concentrator, for example near the end of the concentrator. In general, the magnetic gain at the end of the concentrator is in proportion to the maximum magnetic gain inside the concentrator. The maximum magnetic gain inside the concentrator can be calculated analytically. Eq. (3) is used to calculate its internal field **H**, where the rod is approximated as an ellipsoid with a very long principle axis in x direction and two same length axes in *y* and *z* direction. The N_k is determined by [11]

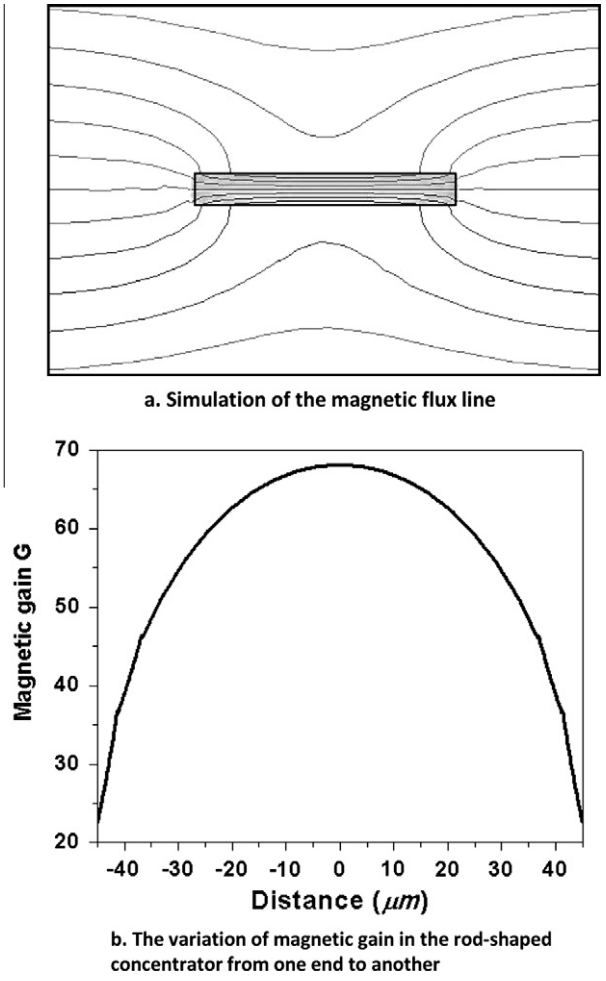

Fig. 1. The simulation results of single rod-shaped concentrator: (a) concentrated magnetic flux lines at the concentrator, (b) magnetic gain as a function of the position from left end to right end of the concentrator.

$$N_x = \frac{4.02\log_{10}(m) - 0.92}{2m^2}, \quad m \geq 10 \tag{4}$$

where *m* is the length-to-diameter ratio (*L*/*d*) of the rod. The maximum magnetic gain inside the rod is defined as $G = \mathbf{B}/\mathbf{B}\_\{0\}$, where the $\mathbf{B}_0 = \mu_0\mathbf{H}_0$ From Eqs. (3) and (4), we can obtain

$$G = \frac{\mathbf{B_x}}{\mathbf{B_0}} = \frac{\mu \mathbf{H}}{\mu_0 \mathbf{H_0}} = \frac{\mu_r}{1 + N_x(\mu_r - 1)} \tag{5}$$

As such, the maximum magnetic gain can be calculated analytically. Therefore, the analytical solution of the maximum magnetic gain is helpful for understanding and analyzing the physical principle of magnetic flux concentration in the vicinity of the MFC, where a MR sensor can be placed.

3. Principles of magnetic flux concentrator

Based on the above analytical model on the magnetic flux concentration of a rod-shaped MFC, the magnetic amplification behaviors of MFCs were studied. The dependences of the magnetic gain of MFC on material, aspect ratio, and shape were analyzed in detail. Since the commercially available MR sensors for magnetic field detection are typically in the size range of micrometer [5], the physical dimensions of MFC studied here are in the micrometer range in order to be compatible with the sensors.

3.1. Materials

Here we investigated the relation between the magnetic amplification and the relative permeability μ_r of the MFC. Considering the scenario of a rod-shaped MFC with flat ends, the maximum magnetic gain can be calculated by using Eq. (5). The maximum magnetic gain is obtained in the center region of the concentrator as discussed above. The variation of the maximum magnetic gain with the relative permeability is plotted in Fig. 2 with three different length-to-diameter ratio m FEM simulations were carried out to validate the results of these analytical calculations. The magnetic gain in the FEM simulation is calculated as the ratio of the maximum magnetic field value inside the MFC to the uniform external magnetic field. It can be seen that the simulation results agree with the corresponding analytical calculation as shown in Fig. 2. It is found that, the maximum magnetic gain is asymptotic to an upper limit as μ_r increases. The upper limit is determined by m and can be calculated from Eq. (5). When the relative permeability tends to infinite, Eq. (5) can be approximated to $G = 1/N_x$ ($m = 20$, $G = 186$; $m = 50$, $G = 843$; $m = 100$, $G = 2809$). That means, in practice, one can obtain higher magnetic gain *G* by using material with a higher relative permeability. However, the upper limit of the *G* is limited by the length-to-diameter ratio m.

Please cite this article in press as: X. Sun et al., Microelectron. Eng. (2013), http://dx.doi.org/10.1016/j.mee.2013.01.063

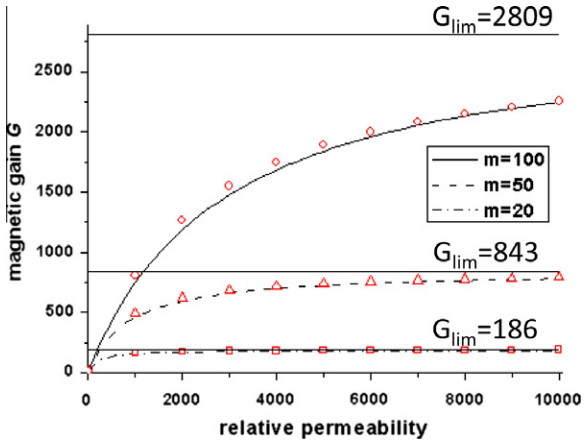

Fig. 2. The magnetic gain G as a function of relative permeability. The analytical calculation result and FEM simulation result are respectively denoted by curves and markers. The upper limit of G is denoted by straight solid line for each m.

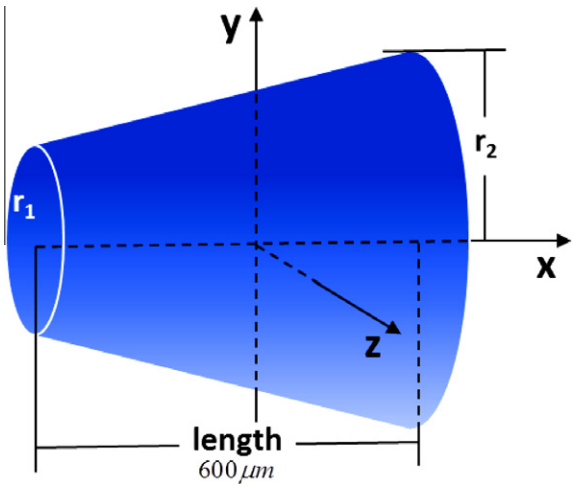

Fig. 4. The geometry of the cone-shaped concentrator.

3.2. Aspect ratio

The relation between the magnetic amplification and the aspect ratio (length-to-diameter ratio m here) was investigated. The variation of the maximum magnetic gain with different m was calculated with Eq. (5) and the result is plotted in Fig. 3. This variation was plotted for different materials (μ_r = 500, 1000, and 2000). It can be observed that the maximum value of magnetic gain G is a function of m. A higher G can be obtained by increasing m. In addition, for a given material, the magnetic gain tends to be asymptotic to an upper limit. Theoretically, this upper limit can be calculated from (4) and (5) by taking $N_x \approx 0$ in the case of very large length-to-diameter ratio. As such, the upper limit of magnetic gain is equal to the relative permeability μ_r. The higher the relative permeability, the larger the upper limit for the magnetic gain. FEM simulations were used to validate the results of the analytical calculations. The simulation results agree with the corresponding analytical calculations as shown in Fig. 3. For practical application, if sufficient space is provided, higher magnetic gain can be obtained by increasing the length-to-diameter ratio m. This characteristic is particularly useful for MR sensors because one can easily achieve m = 100 or even m = 1000 by CMOS technology at micrometer scale.

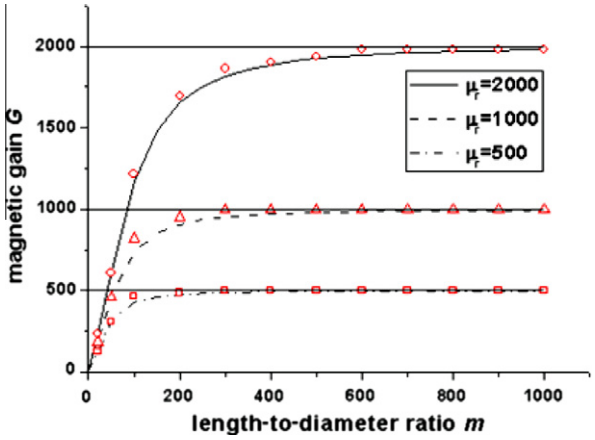

Fig. 3. The magnetic gain G as a function of length-to-diameter ratio m. The analytical calculation result and FEM simulation result are respectively denoted by curves and markers. The straight solid line denotes the upper limit of G for each material.

3.3. Shape

As discussed above, the maximum magnetic gain is obtained at the center of the rod-shaped MFC, which cannot be directly utilized by a MR sensor. A MR sensor is usually placed in the vicinity of the MFC such as near the ends of MFC. In order to improve the magnetic gain in the end regions, the inside maximum magnetic gain needs to be moved from the central region of the concentrator towards the end region near the MR sensor so that a higher magnetic gain can be utilized by the sensor. A cone-shaped MFC is used to illustrate the ideas. The geometry of the cone-shaped concentrator is shown in Fig. 4. It is approximated as a rod-shaped concentrator with one narrower end and one wider end. The ratio between the radius of the wider end r_2 and the radius of the narrower end r_1 is defined as m_r. A 3-D FEM simulation was carried out for computing the magnetic gain of the cone-shaped concentrator with defined length and relative permeability. When one end is narrowed (r_1 reduces and thus m_r increases), the simulation results show that the maximum magnetic gain and its position are functions of m_r as shown in Fig. 5. It can be seen that, as r_1 reduces and m_r increases, the maximum value of magnetic gain increases and its position tends to move closer to the narrowed end. Consequently, a cone-shaped concentrator can provide a higher magnetic gain to the MR sensors than a rod-shaped concentrator. It is because as one end becomes sharper, the maximum magnetic gain increases further and its position also moves from the center towards the sharp

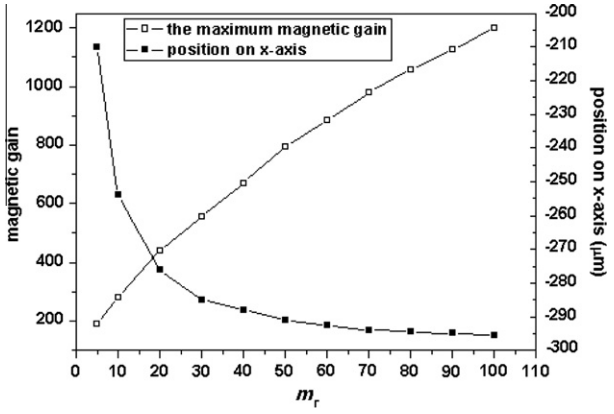

Fig. 5. The maximum magnetic gain G (denoted by open square) and its position (denoted by solid square) as functions of m_r.

Please cite this article in press as: X. Sun et al., Microelectron. Eng. (2013), http://dx.doi.org/10.1016/j.mee.2013.01.063

end. As such, the amplification effect becomes more pronounced at the sharp end.

3.4. Discussion on the parameters for MFC design

3.4.1. Soft magnetic materials

As shown in Fig. 3, with the same length-to-diameter ratio, the MFC made of higher relative-permeability material can achieve higher magnetic gain. In practice, mu-metal (nickel–iron alloys, $\mu_r \approx 10^4$–10^5) and ferrites ($\mu_r \approx 10^3$–10^4) can be used to design MFC. At low frequency, mu-metal can be considered for pursuing higher magnetic gain because the relative permeability of ferrites is weaker. If the sensor operates at a high frequency, the magnetic field noises introduced by these two soft magnetic materials should be considered. At high frequency, the magnetic field noise induced by mu-metal is Johnson current noise due to its high electrical conductivity. The magnetic field noise introduced by ferrites is dominated by the thermal magnetization noise which is weaker than the Johnson current noise introduced by mu-metal. Thus for magnetic field sensing with wide bandwidth, ferrites are preferred rather than mu-metal materials. Although the magnetic field noise somewhat impairs the magnetic gain effects of the MFC, the sensitivity of magnetic sensor is still highly improved by the concentrators without reducing the bandwidth of the sensor [12–14].

3.4.2. Rod length and radius

The larger the length-to-radius ratio, the higher magnetic gain is obtained as shown in Fig. 3, provided material with high enough relative permeability is available. It is also noticed the magnetic gain reaches gradually to a limit as the length-to-diameter ratio increases beyond a certain value. In reality, optimization of the length-to-diameter ratio is also limited by the sensor size and the dimension of the complete system.

3.4.3. Narrowed end

In Fig. 4, the magnetic flux lines converge at the narrowed end of the rod-shaped MFC. It has been shown that a properly shaped MFC can provide very high magnetic gain and modulate the position of the maximum value of the magnetic gain (Fig. 5). As such, a higher magnetic gain can actually be utilized by the sensor than the regular rod-shaped MFC.

4. Design of magnetic flux concentrators

In practice, pairs of concentrators are generally adopted for concentrating magnetic field at the middle gap. As shown in Fig. 6(a), two rod-shaped concentrators are separated by a gap with width g where the magnetic sensor is placed. From the FEM simulation in Fig. 6(b), we can observe that the magnetic flux lines are more concentrated in the gap than the case with a single rod-shaped concentrator in Fig. 1(a). The simulation results show that the magnetic gain in the gap denoted as G_{gap} is inversely proportional to the gap width g.

Due to the limitation of the fabrication techniques, cylindrical shaped MFCs are difficult to be fabricated for MR sensors. Thus cylindrical concentrators can only serve for illustration purposes in this paper, and they cannot be used for intensifying the magnetic field for MR sensors in practice. Here we studied three typical types of concentrators which can be practically fabricated with CMOS process. They are bar-shaped concentrator, T-shaped concentrator, and triangle-shaped concentrator (Fig. 7). Considering a MR sensor with the dimension of 2.0 μm, a pair of MFCs sandwiching a gap $g = 2$ μm where the MR sensor would be installed are simulated. The length L of the MFCs is set to 90.0 μm. The amount of magnetic flux lines are inside the MFC and thus the

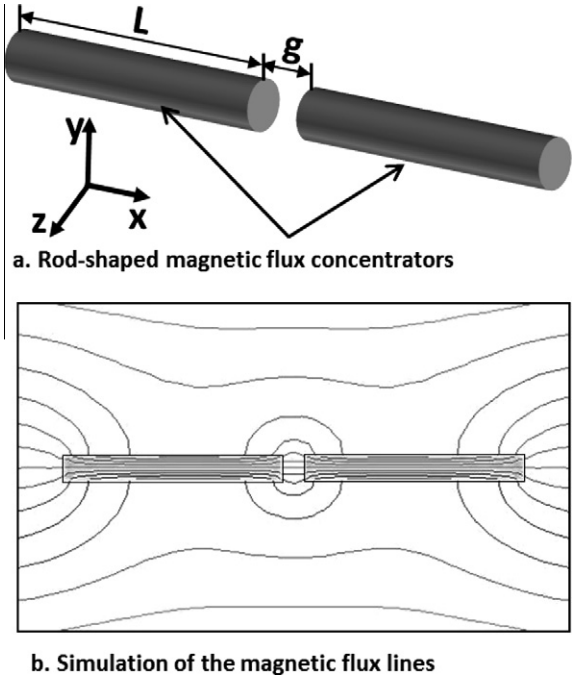

Fig. 6. (a) The geometries of two rod-shaped concentrators. (b) The concentrated magnetic flux lines of two rod-shaped concentrators.

magnetic gain increase with the thickness of the MFC. However, as the thickness increases beyond 2.0 –4.0 μm, the magnetic gain does not increase significantly anymore. When the thickness increases beyond 4.0 μm, the obtained magnetic gain decreases rapidly. Therefore, an optimized MFC thickness is set at 2.0 μm, the same value as the gap width g. The bar-shaped MFCs have a width (w) of 4.0 μm. For the T-shaped and triangle-shaped MFCs, the wide end (w2 = 80.0 μm) is considerably wider than the narrow end (w1 = 4.0 μm). The magnetic gain with w1 = 4.0 μm is about 4% smaller than the maximum magnetic gain obtained with w1 = 2.0 μm. When the width of w1 increases beyond 4.0 μm, the obtained magnetic gain suffers significant decrease. Therefore, the optimized width w1 of 4.0 μm is adopted here in order to provide a uniform amplified magnetic field for the MR sensor. The MFCs are modeled with nickel–iron alloy (mu-metal), which is assumed to be homogenous, linear, and isotropic in our simulation. The relative permeability is set to $\mu_x = 10^4$ at the beginning of its B-H curve. The physical principles of magnetic flux concentration studied in the previous section were applied to the design of these MFCs. With uniform external magnetic field $\mathbf{B}_0 = 1.0 \times 10^{-8}$ - Tesla, 3-D FEM simulations were carried out for studying the magnetic gain, linear working range, and optimized performance.

The magnetic gain versus the external magnetic field is computed and plotted in Fig. 8. As can be seen, the maximum magnetic gains are G = 56 for T-shaped concentrator, G = 51 for triangle-shaped concentrator, and G = 38 for bar-shaped concentrator. The magnetic gain of the T-shaped concentrator remains constant until the relative permeability of the concentrators starts to go into saturation due to the increased external magnetic field. As such, when the external magnetic field is more than 1.6 mTesla, the magnetic gain falls down rapidly. We define the range of the external magnetic field within which the magnetic gain keeps constant as the linear working range of the MFC. Therefore, the linear working range for this T-shape concentrator is 1.6 mTesla. Respectively, the linear working range for triangle-shaped concentrator and bar-shaped concentrator are 3.7 mTesla and 2.6 mTesla. The difference in the working ranges can be explained by an equivalent

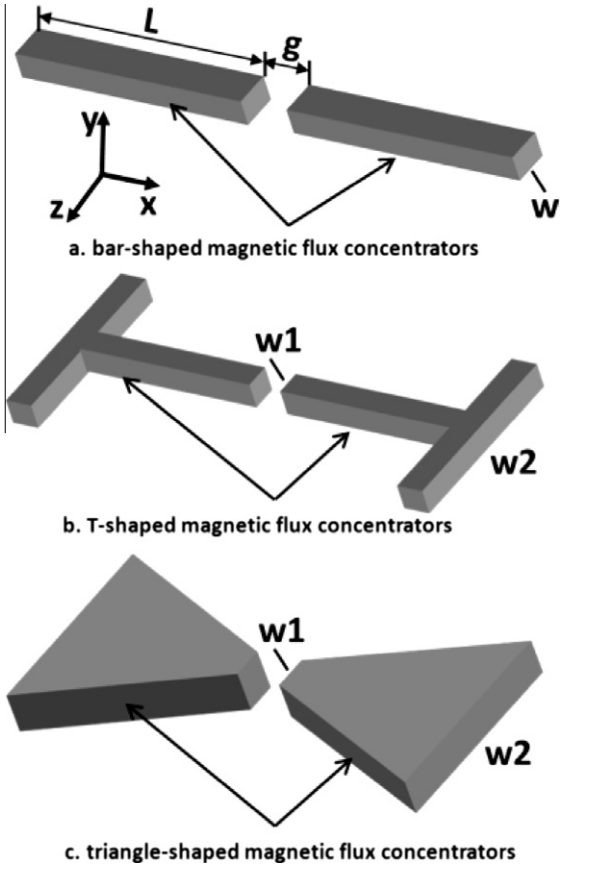

Fig. 7. The geometries of three typical MFCs.

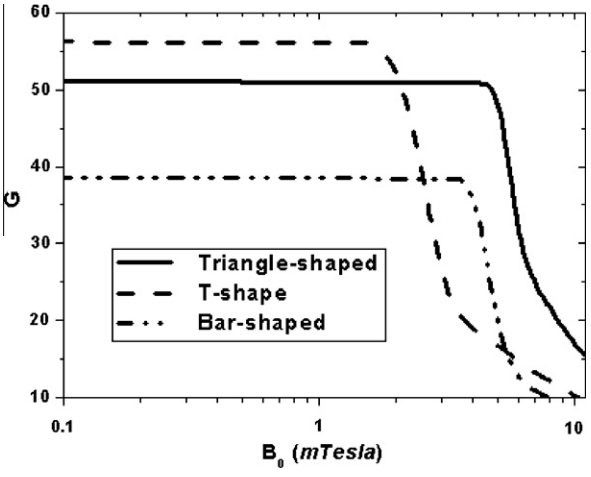

Fig. 8. Magnetic gain versus the external magnetic field for different geometries of MFCs.

magnetic circuit of the pair of concentrators [9]. The narrower parts of the MFCs perform as small magnetic permanence. The magnetic flux lines inside them are even more highly concentrated than the other parts of the MFCs, which can make MFCs with narrower parts saturate earlier than MFCs without narrower parts. Since the geometries of these three types of MFCs are different, their working ranges are therefore different.

The above simulation results show that different type of concentrator can meet different requirement of magnetic flux concentration in practice. For example, since the bar-shaped concentrator is simple in geometry, it alleviates the space constrain and complex fabrication. If high magnetic gain is required, a T-shaped concentrator can be chosen in place of the bar-shaped concentrator. It provides higher magnetic gain but with narrower linear working range than the bar-shaped concentrator. A triangle-shaped concentrator offers magnetic gain which is 10% lower than the T-shaped concentrator but with a wider linear working range than the others.

5. Conclusions

This work presents the study of MFCs for MR sensors as magnetometers to be applied in ultralow field detection. We focused on the magnetic flux concentration in the micrometer dimension. Since the size of MFC can be designed to be considerably larger than the MR sensor at the micro-scale, the geometric parameters of the MFC are critical especially for enhancing the magnetic gain. The magnetic flux concentration principles regarding material, aspect ratio, and shape were investigated. FEM simulations were carried out to verify the analytically studied principles. Based on these principles and simulation results, three typical MFCs were designed for application with MR sensors. Their magnetic gain and linear working range were analyzed and compared. The T-shaped concentrator provides higher magnetic gain of $G = 56$, however, with a narrow linear working range of 1.6 mTesla. The bar-shaped concentrator is compact in size. It provides 32.1% smaller magnetic gain of $G = 38$ but with a medium linear working range (2.6 mTesla) which is 62.5% wider than the T-shaped concentrator. The triangle-shaped concentrator has the widest linear working range (3.7 mTesla, 42.3% wider than the bar-shaped concentrator) and provides a comparable magnetic gain of $G = 51$ with the T-shaped concentrators. As such, this work provides general guiding principles that can be applied in MFC design at the micrometer scale. Based on these principles, optimized MFC can be designed to meet the requirements of field detection application for MR sensors, such as providing high magnetic gain, wide linear working range, compact size, or a tradeoff performance among these requirements.

Acknowledgments

This work was supported in part by the Seed Funding Program for Basic Research from the University of Hong Kong, the RGC-GRF grant (HKU 704911P), the University Grants Council of Hong Kong (Contract No. AoE/P-04/08), and ITF Tier 3 funding (ITS/112/12).

References

[1] H. Beltran, C. Reig, V. Fuster, D. Ramirez, M.D. Cubells-Beltran, IEEE Sens. J. 7 (2007) 1532–1537.
[2] A. Jander, C. Smith, R. Schneider, San Diego, CA, USA, 2005. pp. 1–13.
[3] S. Yamada, K. Chomsuwan, M. Iwahara, in: 5th IEEE Conference on Sensors, 2006, pp. 927–930.
[4] (2011, May 06). Available: http://www.nve.com.
[5] (2012, May 06). Available: http://www.micromagnetics.com/.
[6] A.S. Edelstein, G.A. Fischer, J.E. Burnette, W.E. Egelhoff, S.F. Cheng, IEEE 2009 (2009) 1852–1855.
[7] A.S. Edelstein, G.A. Fischer, J. Pulskamp, M. Pedersen, W. Bernard, S. F. Cheng, in: Proceedings of IEEE on Sensors, vol. 3, 2004, pp. 1562–1565.
[8] A. Guedes, J.M. Almeida, S. Cardoso, R. Ferreira, P.P. Freitas, IEEE Trans. Magn. 43 (2007) 2376–2378.
[9] P.M. Drljaca, F. Vincent, P.A. Besse, R.S. Popovic, Sens. Actuators, A 97–98 (2002) 10–14.
[10] J.A. Osborn, Phys. Rev. 67 (1945) 351–357.
[11] P. Leroy, C. Coillot, A.F. Roux, G.M. Chanteur, IEEE Sens. J. 6 (2006) 707–713.
[12] W.C. Griffith, R. Jimenez-Martinez, V. Shah, S. Knappe, J. Kitching, Appl. Phys. Lett. 94 (2009).
[13] S.K. Lee, M.V. Romalis, J. Appl. Phys. 103 (2008).
[14] J.M. Almeida, P.P. Freitas, J. Appl. Phys. 105 (2009).